

## Performance of the Antiproton Source During Run 1b

Steve Werkema  
September 1995

### Introduction

The most important limitation to the luminosity integrated by the Tevatron collider is the ability to produce and deliver to the collider abundant quantities of antiprotons. The length of time required to accumulate a usable number of antiprotons is a significant factor in the management of collider operations. In this section we discuss the issues relevant to antiproton stacking and issues relating to the transfer of antiprotons to the collider (unstacking).

### I. Stacking

The best reproducible antiproton stacking rate achieved during Run 1b was 7.2 mA/hr for stacks less than 50 mA (1mA =  $10^{10}$  antiprotons). For stacks larger than 50 mA, the "best stacking rate" falls off with increasing stack size at a rate of approximately 1 mA/hr for every 50 mA increase in stack size (see Figure 1). The "best stacking rate" is the rate that is achieved when everything is working well and the antiproton production target is being delivered beam at the maximum intensity and rate (i.e. NTF is not running and there are only antiproton production cycles - \$29's - in the time line). A reasonably accurate, albeit completely empirical, parameterization of the best stacking rate as a function of stack size is given by:

$$R(I) = R_0 \operatorname{sech}\left(\frac{I}{I_m}\right) \quad (1)$$

where  $R$  is the stacking rate,  $I$  is the stack size,  $R_0$  is the stacking rate extrapolated to zero stack size, and  $I_m$  is the stack size at which the stack rate is 64.8% of  $R_0$ . The best stacking of Run 1b is characterized, in this parameterization, by an  $R_0$  of 7.4 mA/hr and an  $I_m$  of 192 mA. This represents an 85% increase in performance relative to that at the beginning of Run 1b.

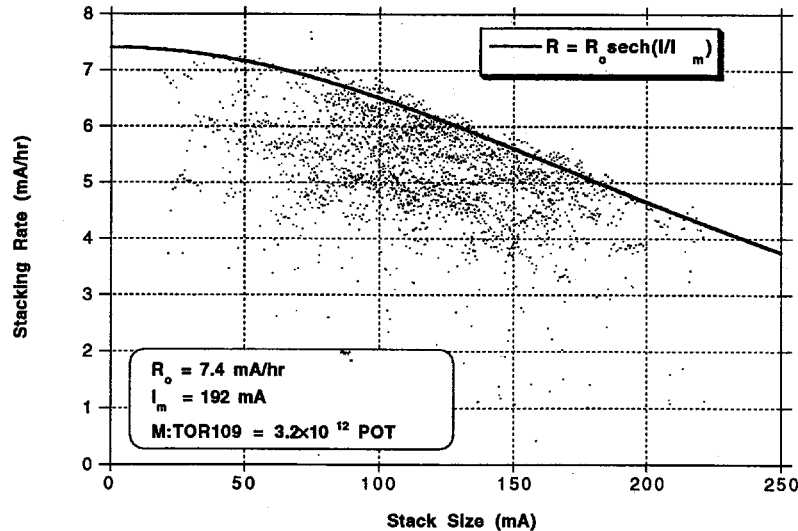


Figure 1. Stacking rate versus stack size for the month of April 1995. One point is plotted for every super cycle during stacking. This month contained the best stacking of Run 1b. POT = Number of protons on target per pulse.

The beginning of Run stacking performance was established in December of 1993 and January 1994. At that time  $\bar{p}$  stacking was characterized by an  $R_o$  of 4.0 mA/hr and an  $I_m$  of 155 mA (Figure 2). The increase in  $R_o$  during the Run is largely due to an increase in the number of protons on target attributable to the Linac upgrade and subsequent Booster improvements [1]. The proton intensity on target at the beginning of the Run averaged  $1.8 \times 10^{12}$  protons/cycle<sup>†</sup>, while at the end of the Run it was  $3.2 \times 10^{12}$  protons/cycle - a nearly 80% gain. The increase in the value of  $I_m$  is due to improvements in the Accumulator which will be discussed later.

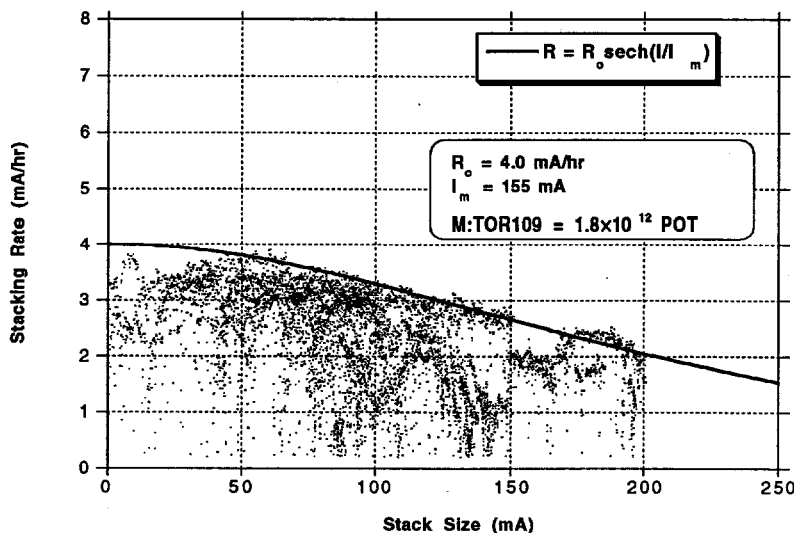


Figure 2. Stacking rate versus stack size for the month of December 1993.

### A. Typical end of Run stacking performance

The rate of antiproton production is the product of the yields and efficiencies associated with every step in the antiproton production chain. Table I gives a summary of several quantities which characterize the stacking performance of the antiproton source.

Table I  
Antiproton Source Stacking Yields and Efficiencies

Protons on target (POT)	$3.2 \times 10^{12}/\text{cycle}$
Antiproton yield into the Debuncher	$21 \times 10^{-6} \bar{p}'s/\text{POT}$
Debuncher to Accumulator transfer efficiency	80%
Stacktail cooling efficiency	90%
Overall antiproton production efficiency	$15 \times 10^{-6} \bar{p}'s/\text{POT}$

A description of each of the items in Table I is given below.

#### Protons on Target

The number of protons on target is measured by a toroid in the AP1 beamline which is located upstream of the target. The ACNET designation of this toroid is M:TOR109.

#### Debuncher Yield

The yield into the Debuncher is the number of antiprotons injected into the Debuncher, as measured by a longitudinal Schottky pickup in the Debuncher (D:FFTTOT), divided

<sup>†</sup> This number is corrected so that it reflects an 11% calibration change in M:TOR109 that was made on 20 January 1995.

by the number of protons on target from M:TOR109. The D:FFTTOT measurement is triggered 350 msec after injection of beam into the Debuncher.

### Debuncher to Accumulator transfer efficiency

The Debuncher to Accumulator transfer efficiency is the fraction of the  $\bar{p}$ 's injected into the Debuncher (D:FFTTOT) that make it into the Accumulator. The number of  $\bar{p}$ 's injected into the Accumulator is measured by a longitudinal Schottky pickup in the Accumulator which is triggered prior to moving the newly injected beam to the stacking orbit. The result of the Accumulator injected beam measurement is stored in ACNET parameter A:FFTTOT. The Debuncher to Accumulator transfer efficiency is the ratio A:FFTTOT/D:FFTTOT.

### Stacktail cooling efficiency

The stacktail cooling efficiency is defined as the fraction of  $\bar{p}$ 's injected into the Accumulator which make it to the core of the Accumulator beam momentum distribution and stay there. This efficiency,  $\epsilon$ , is given by:

$$\epsilon = \frac{R}{A:FFTTOT} T_{\text{cycle}} \quad (2)$$

where R is the stacking rate (A:STCKRT) and  $T_{\text{cycle}}$  is the time interval between Main Ring stacking cycle resets.

### Overall antiproton production efficiency

The  $\bar{p}$  production efficiency is the ratio of the number of  $\bar{p}$ 's stacked in a given time interval to the number of protons striking the production target in that same time interval.

## B. Stacking parameters

There are many tunable parameters in the antiproton source complex that bear directly on stacking. For purposes of documentation, the typical values of a few of the more important parameters are given in Table II.

**Table II**  
**Antiproton Stacking Machine Parameters**

Proton beam spot size on target (sigma)	0.2 mm
Lithium Lens gradient	750 Tesla/m
Debuncher Bunch Rotation RF Voltage	5 MV
Debuncher Stochastic Cooling Power	1100 Watts/plane
Stacktail Momentum Cooling Power	600 Watts
Accumulator Core Cooling Power	30 - 50 Watts
Stacking RF voltage	70 kV
Stacking cycle time	2.4 sec (@ 0 - 50 mA) to 3.8 sec (@ > 180 mA)

## C. Limits to stacking rate

The various factors which limit the rate at which antiprotons can be accumulated and the improvements that have expanded these limits during the course of Run 1b are discussed here.

### 1. Protons on target

Throughout the course of Run 1b there have been frequent step increases in the intensity of the 120 GeV proton beam delivered to the  $\bar{p}$  production target. The  $\bar{p}$  stacking rate has generally followed this increase. We have, however, reached the point at which an increase in the number of protons on target will effect less than the same

percentage increase in  $\bar{p}$  stacking rate. Prolonged running with proton intensities in excess of order  $3 \times 10^{12}$  per cycle has been observed to cause damage to the target [2]. This necessitates the use of a larger beam spot size on the target which in turn lowers the antiproton collection efficiency. Significant upgrades in the target station are being planned to accommodate the much larger proton intensity and shorter cycle time envisioned when the Main Injector becomes operational.

### 2. Debuncher stochastic cooling

The efficiency with which  $\bar{p}$ 's are transferred from the Debuncher to the Accumulator depends critically on the transverse beam size after cooling in the Debuncher (see Figure 3). There is as much as a 10% loss of beam during transfer which would be avoided if the  $\bar{p}$  emittances prior to transfer were made smaller. At the present time the Debuncher stochastic cooling system is power limited; that is, the system must be operated at a gain setting which is less than the optimum gain to maintain the output power below a level at which damage to the kicker hardware occurs. Thus, the final emittance achieved prior to transfer to the Accumulator is determined entirely by the emittance of the beam injected at the beginning of the cycle. The only way, during run 1b, to further decrease the Debuncher beam size prior to extraction is to increase the stacking cycle time, allowing more time for cooling. Increasing the cycle time, particularly for large stacks, also increases the stacktail cooling efficiency in the Accumulator. However, only small increases in cycle time are beneficial. The increase realized in Debuncher to Accumulator transfer efficiency and stacktail efficiency will quickly be overcome by the loss of flux from the target due to fewer proton pulses on target per unit time, thus compromising the overall stacking rate. Figure 3 illustrates the effect of cycle time on Debuncher to Accumulator transfer efficiency and Debuncher emittances.

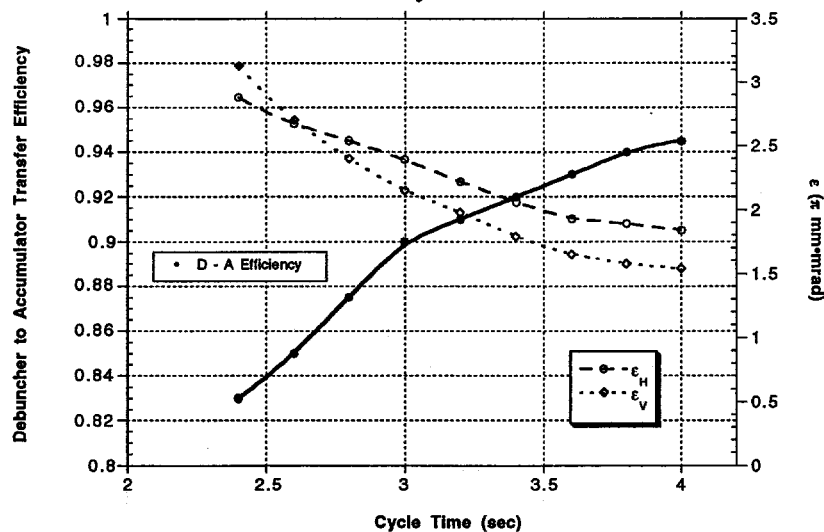


Figure 3. Debuncher to Accumulator transfer efficiency and Debuncher emittances as a function of stacking cycle time. The emittances are measured using a SEM grid in the D-A transfer line (SEM 806). The emittance values plotted in this figure are not normalized. This Figure was taken from reference [3].

### 3. Stacktail momentum cooling

During stacking the Accumulator functions as follows: Beam from the Debuncher is injected, using a shuttered kicker, onto an orbit at the high energy side of the momentum aperture of the Accumulator. The newly injected beam is decelerated with a 53 MHz ( $h = 84$ ) RF system (ARF1) to the stacking orbit - an orbit near the center of the momentum aperture. The beam is then stochastically cooled into the existing  $\bar{p}$  stack with the stacktail momentum cooling system.

There was a significant amount of effort during Run 1b devoted to understanding and improving the Accumulator stacktail momentum cooling system. There are two issues which have determined how the stacktail system is operated. First, the gain must be high enough (or the stacking cycle time long enough) to allow the stacktail momentum cooling to move freshly deposited beam off of the stacking orbit prior to the arrival of the next pulse. Any beam remaining on the stacking orbit will be phase displaced backwards, to a higher energy, by ARF1 during the next cycle. Subsequent stacking cycles will eventually cause this beam to be accelerated into the injection kicker shutter. The second issue is transverse and longitudinal heating of the beam at the core of the  $\bar{p}$  momentum distribution by the stacktail momentum cooling. In general, the higher the gain setting of the stacktail momentum cooling, the greater the heating of the core will be. A considerable amount of progress was made in mitigating both of these issues during the course of Run 1b.

The rate at which freshly deposited antiprotons move into the  $\bar{p}$  stack is determined by the stacktail momentum cooling gain profile and the shape of the  $\bar{p}$  momentum distribution in accordance with the Fokker-Plank equation [4]. The stacktail momentum cooling system consists of a high energy and a low energy pickup connected via independent networks of gain and delay to a common set of kickers. Ideally the high and low energy legs function independently. The high energy leg serves to move newly deposited  $\bar{p}$ 's off of the stacking orbit while the low energy leg functions primarily to move beam from the stacktail into the core. When the system functions in this manner the total power put onto the beam by the stacktail momentum kickers at any time in the stacking cycle is minimized. The gain profile of the combined system is the vector sum of the high and low energy legs. The overall stacktail momentum cooling gain profile can be tuned by manipulating the gains and delays of the individual legs.

In its design configuration, the high energy pickup was located 16 MeV above the central orbit and the low energy pickup was located 1 MeV below the central orbit. In this configuration there is a significant overlap in the response of the two pickups with the result that the high energy and low energy legs act largely to cancel each other.

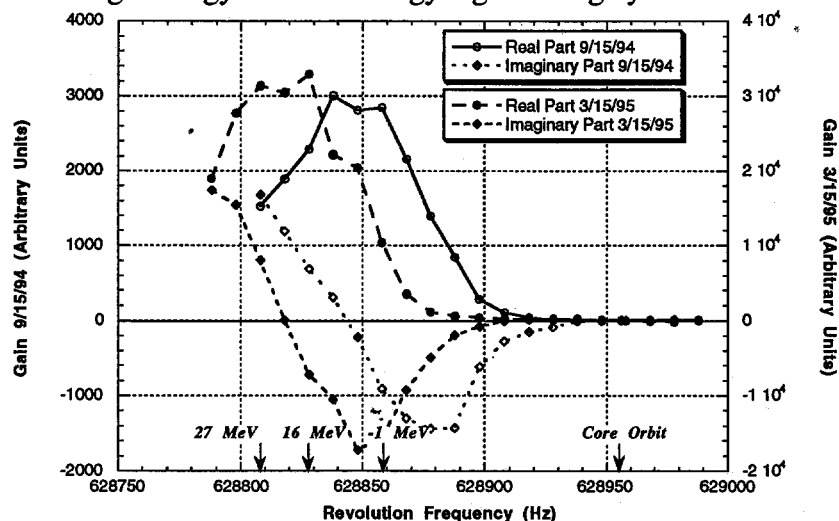


Figure 4. Real and imaginary parts of the stacktail cooling gain profile before and after the hardware changes of Run 1b. The quantity measured here is the response of the stacktail cooling system to a delta function of beam at each revolution frequency. It is the real part of the gain that moves the beam toward the core. The approximate factor of 10 difference in the gain scales between the 9/25/94 measurements and the 3/15/95 measurements is due, in part, to differences in the way the data was normalized.

In November of 1994 the high energy pickup was moved to 27 MeV above the central orbit. The effect of this move was to separate the two pickups by a distance greater than the width of the individual pickup response. This move permitted moving the peak in the system response farther from the core allowing more stacktail system gain for the same amount of core heating [5].

Even with increased separation of the high and low energy pickups there remained a significant response in the -1 MeV leg to beam on the stacking orbit. This undesirable response was largely eliminated by re-commissioning the -23 MeV compensation leg of the stacktail momentum cooling system. The -23 MeV leg consists of a pickup, located 23 MeV below the momentum of the central orbit, connected via gain and delay into the -1 MeV leg. This leg was originally intended to correct the response of the -1 MeV leg to beam near the core orbit. However, the -23 MeV leg is currently phased to correct the response of the -1 MeV leg to beam near the stacking orbit [6].

The -23 MeV compensation leg also serves to correct the response of the -1 MeV leg to *horizontal* beam motion at the core momentum. The -1 MeV pickup is sensitive to the horizontal betatron motion of the beam at the core (the pickups are horizontally opposed, thus vertical motion is not detected). The relatively large number of particles at the core give rise to a strong signal at the horizontal betatron sideband frequencies of the core. The -1 MeV leg of the stacktail momentum cooling system responds to this signal by putting power on the stacktail kickers at the betatron sideband frequencies within the stacktail momentum cooling bandwidth. While the kick to the beam is primarily longitudinal, imperfections in the system (which will be enumerated in the next section) couple some of this power into the horizontal plane. The result is horizontal heating of the beam at the core. The -23 MeV pickup, due to its close proximity to the core, is also sensitive to the horizontal motion of the core. It turns out that when the -23 MeV compensation leg is phased to correct the longitudinal response at the stacking orbit it also provides a 10 to 15 dB reduction in the response of the -1 MeV leg to the horizontal motion of the core [7].

In addition to the high energy pickup move and -23 MeV leg re-commissioning, there was a substantial amount of activity directed to measuring and characterizing the performance of stacktail momentum cooling in the Accumulator. These efforts included a series of measurements which allow a complete characterization of the system for purposes of computer modeling. The net effect of all of these improvements was to accommodate the increased  $\bar{p}$  flux through the system without further exacerbating the core heating. Figure 4 illustrates the evolution of the stacktail momentum gain profile over the course of Run 1b.

#### *4. Core heating by the stacktail cooling*

As was indicated previously, the stacktail momentum cooling heats the beam at the core of the momentum distribution. The amount of core heating increases as the  $\bar{p}$  stack grows. Moreover, the effectiveness of the core stochastic cooling systems decreases as the stack size increases. The heating is the result of the core being driven transversely by the stacktail cooling system at the betatron sideband frequencies of the core. The transverse kick comes from mechanical misalignment of the stacktail cooling kicker electrodes, residual dispersion in the Accumulator lattice at the kicker locations, and small difference signals applied to the momentum kicker electrodes due to imperfect hybrids. Core heating from the stacktail momentum cooling system is one of the reasons the stacking rate declines as the stack size increases.

This transverse heating is partially compensated for by horizontal and vertical  $\Delta$  kicker hardware installed on five of the sixteen stacktail momentum kickers. The  $\Delta$  kickers allow the application of a variable transverse kick by the kickers on which they are installed by applying a difference signal to the kicker electrodes in addition to the normal sum signal which provides the longitudinal kick. The transverse kick from the  $\Delta$  kickers is adjusted to approximately cancel the spurious transverse kicks from all of the other kickers.

The  $\Delta$  kickers work well, however, this correction is not perfect. The  $\Delta$  kicker correction is optimized for revolution frequencies near the core of the  $\bar{p}$  momentum distribution (revolution frequency of 628955 Hz). There is a region of significant heating at a revolution frequency of 628930 Hz where the  $\Delta$  kicker correction is much less effective (see Figure 5).

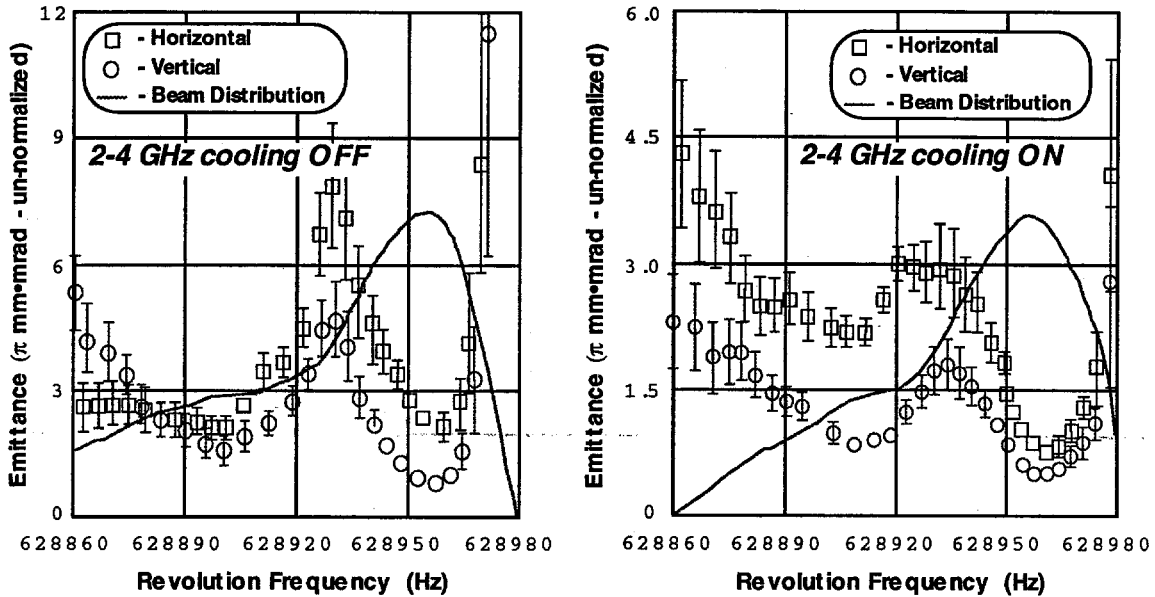


Figure 5. Effect of the 2-4 GHz transverse core cooling system on overcoming the emittance growth due to heating from the stacktail momentum cooling at a revolution frequency of 628930 Hz. The stack size in each case was 135 mA. Note that the vertical scale on the right hand plot is expanded by a factor of two relative to the left-hand plot.

The solution implemented in Run 1b was to install a second core transverse cooling system for each transverse plane. The transverse core cooling configuration at the beginning of the Run was a single 4-8 GHz system for each plane. In March of 1995 the existing transverse cooling hardware was modified to include 2-4 GHz pickups and kickers. The lower frequency cooling extends the revolution frequency range over which the cooling electronics is phased to the beam. For a maximum phase error of  $\pm 60^\circ$  (i.e. the error at which the cooling gain is attenuated by  $\cos(\pi/3) = .5 = 6\text{dB}$ ), the range of revolution frequencies ( $\Delta f_{rev}$ ) at which effective cooling will occur is given by:

$$\Delta f_{rev} < \frac{f_{rev}^2}{3\alpha f_{max}} \quad (3)$$

where  $f_{rev}$  is the core revolution frequency,  $f_{max}$  is the upper end of the cooling band width and  $\alpha$  is the fraction of the total circumference of the accelerator which comprises the distance from the cooling pickup to the kicker. For the Accumulator core cooling systems  $\alpha$  is  $1/3$ . For the 4-8 GHz system  $\Delta f_{rev}$  is 50 Hz centered at the core. With only the 4-8 GHz transverse cooling the cooling gain is attenuated by 3dB at 628930 Hz. The

2-4 GHz system extends this down to a revolution frequency of 628905 Hz, which completely contains the region of increased beam heating.

Subsequent to the commissioning of the Accumulator transverse 2-4 GHz cooling the value of  $I_m$ , in the stacking parameterization of equation (1), increased from a value of approximately 150 mA<sup>†</sup> to 192 mA.

### 5. LCW temperature

The antiproton source magnets, power supplies, RF system high power amplifier tubes, and the stochastic cooling traveling wave tubes are cooled by a low conductivity water (LCW) cooling system. It has been observed that the antiproton stacking is degraded when LCW temperatures rise. Figure 6 shows a slight decline in average stacking rate when the LCW supply temperature exceeds 85°F with a more pronounced decline when the LCW supply temperature goes above 92°F.

This effect is not yet completely understood. It is well known that the LCW temperature affects the integrated bend field and quadrupole gradient (magnets expand and contract and pole spacings change). However, since field and gradient changes are routinely compensated for with bend bus adjustments and tune corrections, it is likely that something else is adversely affecting the antiproton source when the LCW system gets hot.

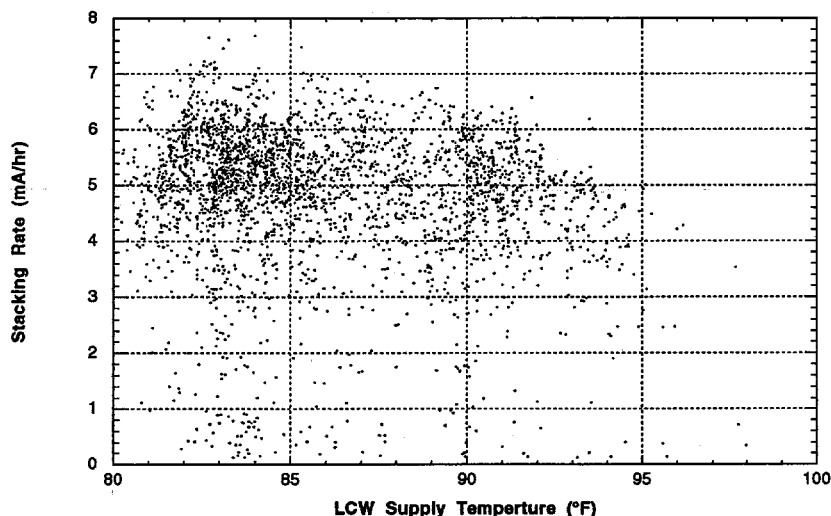


Figure 6. Antiproton stacking rate versus LCW supply temperature for the period from 1 March 1995 through 24 July 1995.

<sup>†</sup> This value of  $I_m$  is determined from the stacking performance of January 1995.

## II. Unstacking

Unstacking is the process by which antiprotons are extracted from the Accumulator core and transferred to the Main Ring for acceleration and injection into the Tevatron. The beam at the Accumulator core is bunched at twice its revolution frequency by a single bucket (or suppressed bucket) RF system. The bunched beam is accelerated to the extraction orbit of the Accumulator where it is kicked by means of a shuttered kicker into the AP3 beamline for transfer to the Main Ring.

### A. Amount of beam unstacked

The goal of this process is the transfer of the maximum possible number of  $\bar{p}$ 's into the Tevatron. The following three factors limit the number of  $\bar{p}$ 's which can be transferred:

(1) The maximum RF bucket area which can be used is constrained by the momentum aperture of the Main Ring. The largest bucket area used this Run was 1.55 eV $\cdot$ sec.

(2) The amount of beam contained in a RF bucket of a given size is determined by the longitudinal phase space density of the beam being bunched. The maximum achievable longitudinal phase space density is determined by the capacity of the core momentum cooling and the onset of longitudinal instabilities. Figure 7 shows the longitudinal phase space densities achieved as a function of stack size during Run 1b.

(3) The transfer efficiency of the  $\bar{p}$ 's from the Accumulator core into the Main Ring and beyond is maximized when the transverse emittances of the extracted beam are maintained less than the admittance of the beam lines and the Main Ring. The minimum achievable  $\bar{p}$  transverse emittance is a function of the stack size. This dependence is due to the existence of transverse beam heating mechanisms for which the heating rate becomes greater with an increasing number of beam particles. Therefore, the equilibrium emittances (i.e. when the cooling rate equals the combined heating rate from the various sources of beam heating) increase with increasing beam intensity. Figure 8 shows the dependence of the minimum transverse emittance and momentum spread on  $\bar{p}$  intensity.

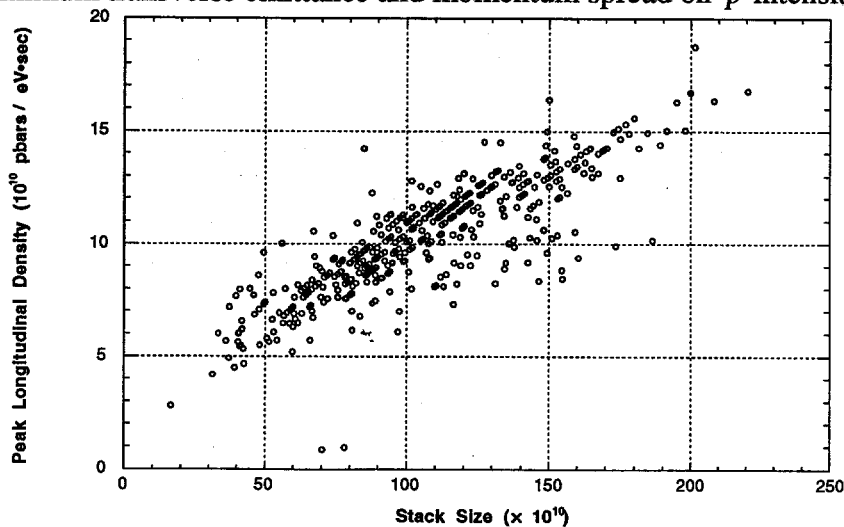


Figure 7. Longitudinal phase space density at the peak of the antiproton momentum distribution just prior to unstacking as a function of stack size.

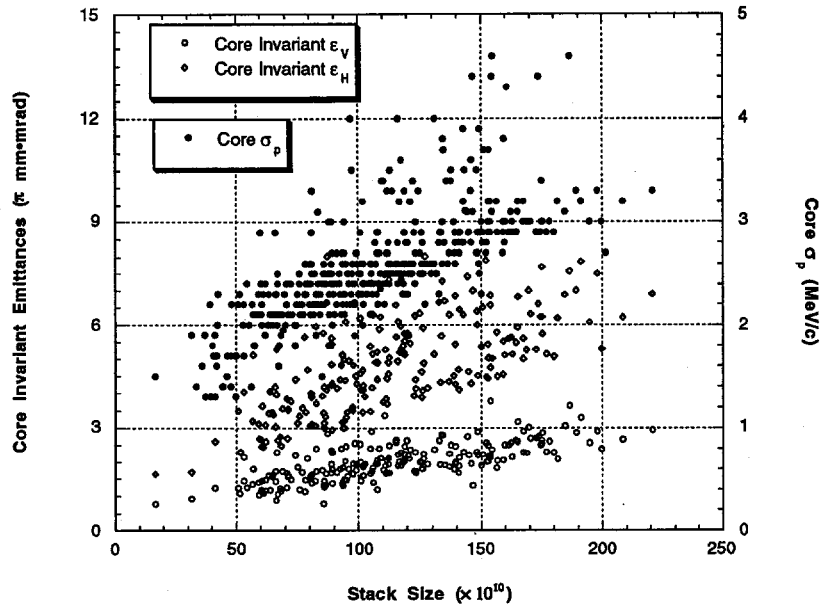


Figure 8. Accumulator core beam size prior to unstacking. In general, the beam is cooled in each dimension to the smallest size possible prior to initiating antiproton transfers.

During the course of Run 1b a variety of RF bucket areas were used for unstacking. The fraction of the antiproton stack extracted as a function of stack size for each size RF bucket is shown in Figure 9. Figure 9 shows that the fraction of the  $\bar{p}$  stack which is removed during the course of unstacking decreases with increasing stack size. This is essentially a consequence of the fact that the momentum spread of the beam increases with increasing stack size (see Figure 8).

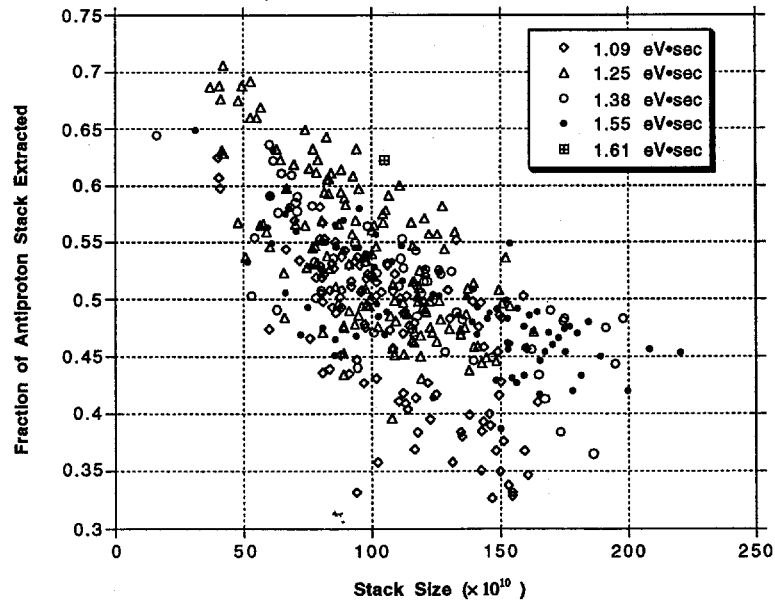


Figure 9. Fraction of Accumulator beam unstacked as a function of stack size for different RF buckets. Note the suppressed zero on the vertical axis.

An approximate understanding of the functional dependence of the amount of beam extracted on RF bucket area and momentum spread can be gained by considering the simple case of a beam with a gaussian momentum distribution being bunched at the

center of the distribution. In this case, for a beam distribution of width  $\sigma_p$ , the fraction,  $\delta N/N$ , of the stack extracted by bunching the beam with an RF bucket area  $B$ , is given by:

$$\frac{\delta N}{N} = \text{erf} \left( \frac{f_{\text{rev}} B}{\sqrt{8} \sigma_p} \right) \quad (4)$$

For the range of bucket areas (0.5 eV•sec to 1.6 eV•sec) and momentum spreads (1.2 MeV/c to 4.0 MeV/c) relevant to  $\bar{p}$  unstacking, the fraction unstacked on a single transfer is approximately linear in the quantity  $B/\sigma_p$ .

From Figure 8 it is seen that  $\sigma_p$  increases by approximately 40% as the stack size increases from  $50 \times 10^{10}$  to  $150 \times 10^{10}$ . The corresponding decrease in  $\delta N/N$  exhibited in Figure 9 is about 30 - 40%, which is in approximate agreement with what is expected from the simple model of equation (4).

One would also expect from equation (4) that an increase in RF bucket area from 1.09 eV•sec to 1.55 eV•sec should yield about a 40% increase in the number of  $\bar{p}$ 's unstacked. From Figure 9 it is clear that this was not the case during Run 1b. This discrepancy is not well understood. There are several possible explanations: (1) the unstacking RF voltage calibration is not known and/or changes with time, (2) beam is expelled from the RF bucket by some unknown mechanism on its way to the extraction orbit (about a 10% loss of beam from the bucket is normal) - the transverse dampers are particularly suspect here, (3) interference from the ion clearing RF system, or (4) errors in measuring the beam momentum distribution. Measurements have been made to investigate all four of these possible problems with no clear resolution of the issue.

## B. Other unstacking issues

During the course of Run 1b there have been a variety of issues which have adversely affected the quantity and quality of the  $\bar{p}$ 's delivered to the collider from the antiproton source. These issues are briefly documented here.

### 1. Transverse emittance growth from the Accumulator core to Main Ring 8 GeV

The most serious unstacking issue is that of  $\bar{p}$  emittance preservation. There is a severe growth in the  $\bar{p}$  transverse emittance during the transfer of antiprotons from the Accumulator core to the Main Ring. The issue is somewhat obscured by uncertainties in the emittance measurements in the Accumulator and in the Main Ring. It is clear however, that given even the most pessimistic uncertainties in the various emittance measurements, a serious dilution of transverse phase space takes place during  $\bar{p}$  transfers. Figure 10 illustrates the problem.

In Figure 10 the vertical plane exhibits an emittance growth which is proportional to the initial Accumulator core emittance. This growth is at least a 4-fold increase in vertical emittance. Also shown is a  $4\pi$  horizontal blowup which is independent of the Accumulator core horizontal emittance. The source of the various kinds of emittance growth can be isolated to some extent by using a beamline SEM grid to measure the emittance of the beam just after it is extracted from the Accumulator. The SEM used for this purpose (SEM 900) is approximately 2 meters downstream of the Accumulator and upstream of any beamline elements. Figure 11 compares the emittances derived from the SEM profile with the Accumulator core emittances.

A comparison of Figures 10 and 11 shows that, if the measurements are taken at face value, most of the vertical emittance growth occurs in the Accumulator. It is also apparent that the horizontal blowup most likely occurs on injection into the Main Ring.

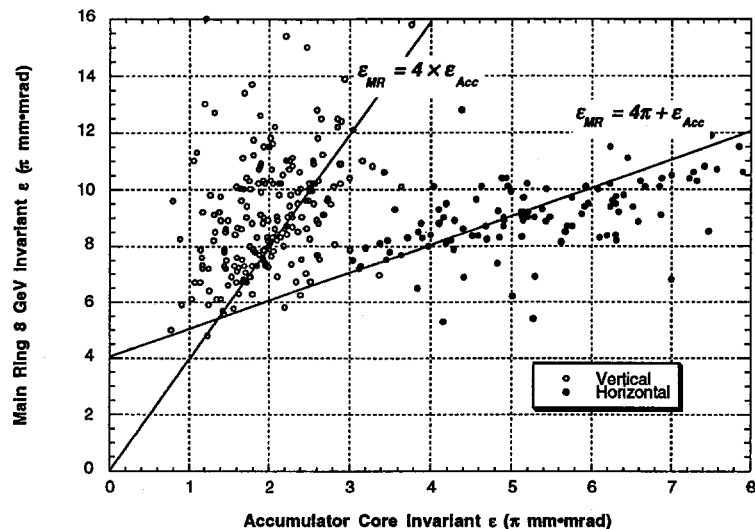


Figure 10. Main Ring flying wire emittances at 8 GeV versus Accumulator core emittances. Main Ring vertical emittance is plotted against Accumulator vertical emittance and Main Ring horizontal emittance is plotted against Accumulator horizontal emittance. The Accumulator emittances are measured using transverse Schottky pickups. Each point in these plots represents the average of all antiproton transfers during the course of a shot (usually 6 transfers). The solid lines indicate that the vertical emittance blows up by at least a factor of 4 while the horizontal emittance growth is  $4\pi$  mm·mrad independent of initial emittance. Some of this  $4\pi$  offset could be measurement error.

The proportional vertical growth shown in Figure 11 is due, in part, to coupling on the Accumulator extraction orbit. Additionally, since Accumulator transverse emittances are correlated with stack size (see Figure 8), some component of this growth may be a  $\bar{p}$  intensity dependent effect.

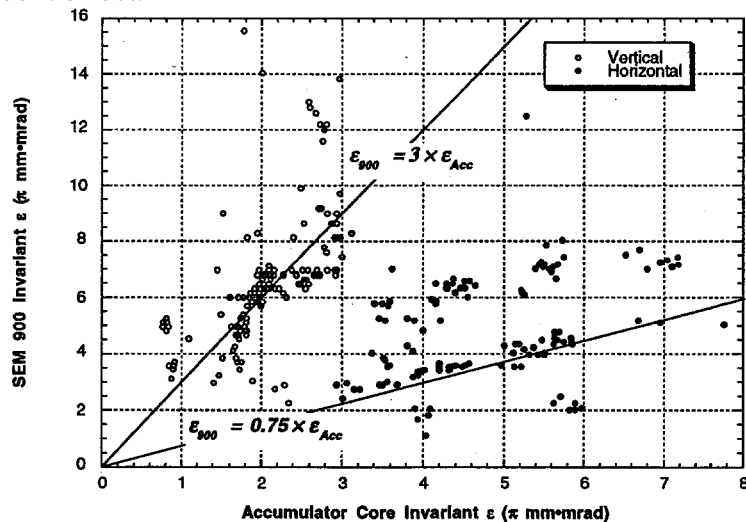


Figure 11. Measured emittances at SEM 900 at the upstream end of the AP3 beamline versus Accumulator core emittances. SEM 900 vertical emittance is plotted against Accumulator vertical emittance and SEM 900 horizontal emittance is plotted against Accumulator horizontal emittance. The data shown here was taken during the period from 17 April 1995 to 23 July 1995. Each point represents a single antiproton transfer.

The unstacked beam spends about 8 sec on the extraction orbit prior to being extracted into the AP3 beam line. Since the extraction orbit lattice is coupled, there should be a time, well before the extraction event, when the horizontal and vertical emittances become equal. If the transverse phase space of the unstacked beam is not diluted in the

accumulator, the horizontal and vertical emittances on the extraction orbit prior to extraction should each be equal to the average of the horizontal and vertical emittances at the core. Therefore, if there is no emittance dilution in the accumulator, and using the fact that, at the core, the vertical emittance is approximately  $\frac{1}{2}$  the horizontal emittance (see Figure 8) the following relationship between extraction orbit and core orbit emittances is expected:

$$\epsilon_H(extr) = \frac{3}{4} \epsilon_H(core)$$

$$\epsilon_V(extr) = \frac{3}{2} \epsilon_V(core)$$

The observed vertical growth is about twice what is expected. The assumption that there is no emittance dilution from core to extraction orbit is not valid. The cause of this vertical growth is not known. The SEM 900 horizontal measurement indicates that about half the time the horizontal growth is consistent with the no dilution hypothesis. This is difficult to understand in light of the coupling on the Accumulator extraction orbit. The observation that, frequently, little or none of the vertical growth is coupled into the horizontal plane may be an indication that the blow up occurs very close to the time of extraction (i.e. within hundreds of beam turns of the extraction event). The relationship between vertical and horizontal emittances at the Accumulator core and extraction orbits and at 8 GeV in the Main Ring are shown in Figure 12.

The horizontal emittance growth on injection into the Main Ring could be the result of an injection steering error or a mismatch in horizontal dispersion. Injection oscillations are normally corrected to an amplitude of less than 1 mm; thus contributing less than approximately  $0.3 \pi$  to the horizontal emittance offset. A large part of the balance of the horizontal growth is likely due to a horizontal dispersion mismatch between the AP1 beamline and the Main Ring. There were several attempts to correct this mismatch with some success; however the mismatch was not completely eliminated due to the difficulty in simultaneously correcting the dispersion and maintaining the  $\beta$ -function match.

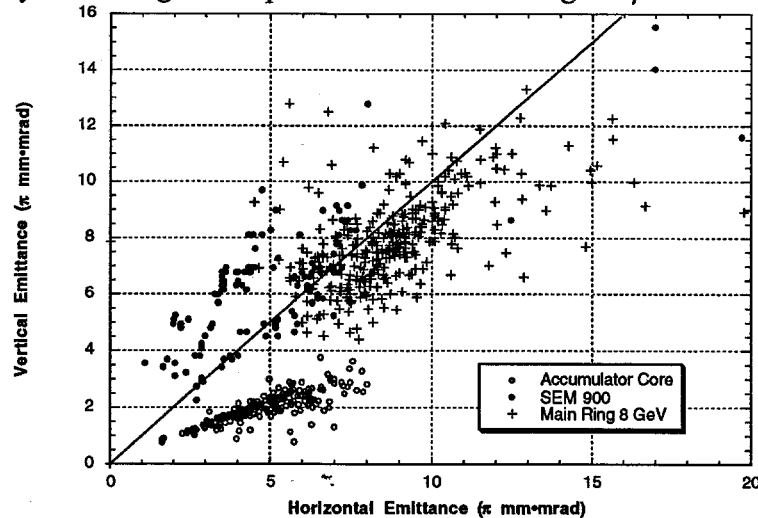


Figure 12. Vertical emittance versus horizontal emittance at the Accumulator core, SEM 900, and Main Ring at 8 GeV. The core and Main Ring data are averages over all transfers in a shot and represent all of Run 1b (i.e. the same data displayed in Figure 10). The SEM 900 data represent individual antiproton transfers during the period 17 April to 23 July 1995 (i.e. the same data displayed in Figure 11).

Finally, it should be noted that the Main Ring 8 GeV lattice is coupled. It is therefore expected that, since beam circulates several hundreds of turns prior to the emittance



system used for ion clearing (ARF2) is the same system currently used for unstacking  $\bar{p}$ 's during a collider fill. The difficulty with this arrangement occurs at those times during the preparation for unstacking  $\bar{p}$ 's when ARF2 must be switched off to program it for its unstacking sequence. If the stack is large, the beam will begin to oscillate transversely. This oscillation often results in rapid growth in the core emittances. If the emittance growth is large enough, time will have to be taken to re-cool the beam; a process usually requiring about 15 to 20 minutes. Bunching with ARF2 during unstacking will stabilize the beam; however, as soon as the unstacked beam is moved away from the core the transverse oscillation of the beam returns (see Figure 13).

The implementation of RF ion clearing was modified to avoid the conflicts associated with using ARF2 for both unstacking and ion clearing. The new scheme has become known as CW RF ion clearing. CW RF ion clearing is simply the use of a signal generator in place of the ARF2 low level electronics during those times when ARF2 is also being used for unstacking. The CW RF signal generator is tuned to twice the revolution frequency of the beam at the core of the  $\bar{p}$  distribution and drives the ARF2 cavities through the final power amplifiers in the ARF2 system. In the sequence shown in Figure 13, the CW RF is switched off 1 sec after the initiation of the unstacking sequence, and is switched on again 7 sec after the start of the sequence until the end of the sequence. The timing of the CW RF was varied extensively during the remainder of Run 1b.

CW RF ion clearing successfully inhibited coherent oscillation of the beam during unstacking; however it is possible that CW RF interferes with unstacking and may be responsible for at least part of the discrepancy between the actual and expected unstacking yield identified above. Measurements performed to test this suspicion have been inconclusive.

### III. Reliability

Any disruption in the operation of the antiproton source has a direct impact on the integrated luminosity of the collider. Lengthy downtime due to equipment failure frequently precludes antiproton stacking thereby reducing the number of antiprotons which are available for transfer to the collider. Failures which cause the loss of the antiproton stack are especially egregious due to the long time it takes to accumulate a sufficient number of  $\bar{p}$ 's for a new collider store (about 10 to 12 hours). The operations department maintains records of all system downtime. Additionally, a concerted effort is made to determine the cause of each stack loss. We present here a summary of the antiproton source reliability data collected during Run 1b.

#### A. Lost Stacks

During Run 1b a total of 70 antiproton stacks were lost with an average interval between lost stacks of 8.2 days. These stack losses caused an accumulated loss of  $4.181 \times 10^{13}$   $\bar{p}$ 's. The causes for these stack losses fall into several categories as indicated in Figure 14.

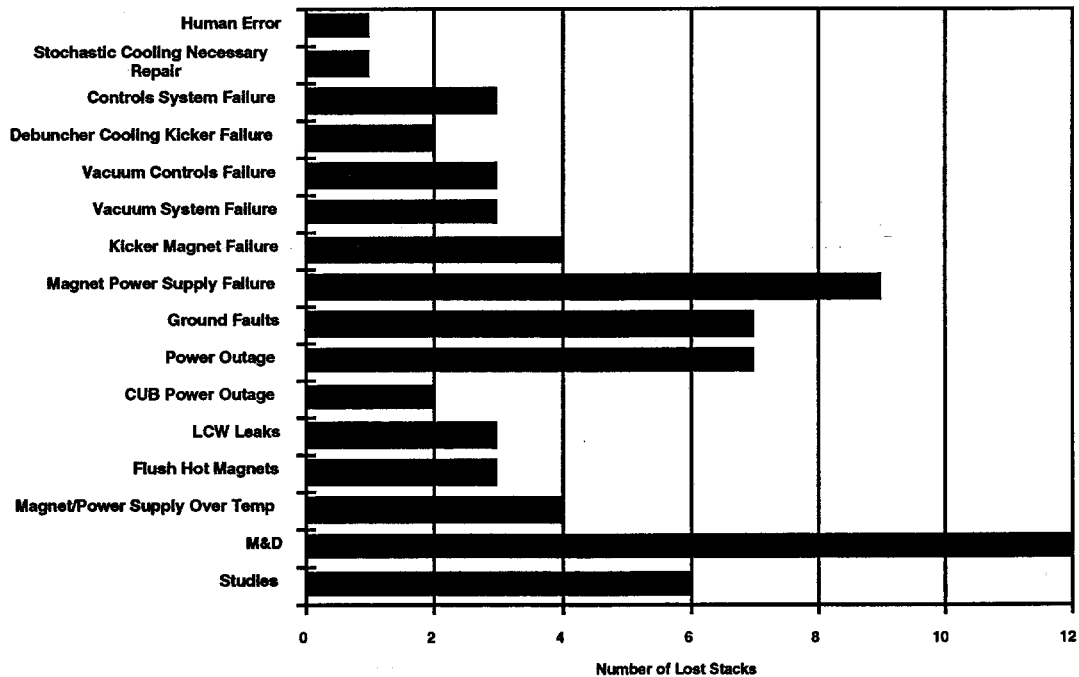


Figure 14. Causes of lost antiproton stacks.

In order to appreciate the value of what has been lost here, it is useful to note that the total antiproton accumulation for Run 1b was  $31.680 \times 10^{13}$   $\bar{p}$ 's of which  $26.318 \times 10^{13}$   $\bar{p}$ 's were unstacked for use in the collider. Thus, lost stacks consumed 13.2% of the total  $\bar{p}$  yield for the Run while 83.1% was used for the collider. The remaining 3.7% of the Run 1b  $\bar{p}$  production consists of failures which caused only a partial loss of the stack as well as special tests (e.g. test shots) which consumed some but not all of the stack.

#### B. Downtime

There were a total of 917 hours of antiproton source downtime during Run 1b, which constitutes approximately 7.2% of the total available running time during Run 1b. Downtime is recorded for the antiproton source whenever the normal scheduled operation of

the antiproton source is interrupted. Scheduled operations for the antiproton source include stacking, shot setup, accelerator studies, and shutdowns for maintenance and development. On each occurrence of downtime, the duration of the downtime is logged and the general category into which the failure which caused the downtime is recorded. A summary of the downtime for Run 1b is given in Figure 15. The definitions of the various categories are given in table III.

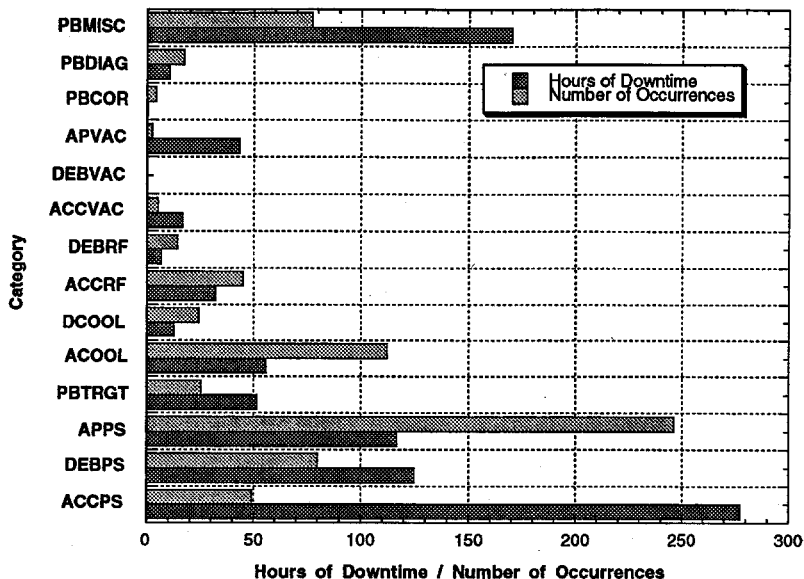


Figure 15. Summary of the antiproton source downtime for Run 1b.

**Table III**  
**Antiproton Source Downtime Categories**

<b>PBMISC</b>	Everything that doesn't fit into another category
<b>PBDIAG</b>	Diagnostic systems
<b>PBCOR</b>	Antiproton source correction elements
<b>APVAC</b>	AP1, AP2, or AP3 beamline vacuum system
<b>DEBVAC</b>	Debuncher vacuum system
<b>ACCVAC</b>	Accumulator vacuum system
<b>DEBRF</b>	Debuncher RF systems
<b>ACCRF</b>	Accumulator RF systems
<b>DCOOL</b>	Debuncher stochastic cooling systems
<b>ACOOL</b>	Accumulator stochastic cooling systems
<b>PBTRGT</b>	Antiproton source target station systems
<b>APPS</b>	Beamline power supplies and magnets
<b>DEBPS</b>	Debuncher power supplies and magnets
<b>ACCPS</b>	Accumulator power supplies and magnets

One common source of downtime during Run 1b was magnet over-temperature trips. When a magnet overheats an interlock trips the power supply to the bus supplying that magnet. The interlock resets when the magnet has sufficiently cooled to safely restore power to the bus. This cool down typically takes 15 - 30 minutes. This type of failure spans several of the categories shown in Figure 15. The total time lost due to magnets overheating during Run 1b was 97 hours, or about 10.5% of the total downtime for the antiproton source. The underlying cause of the large number of overheating magnets in the antiproton source is the build up of copper oxide in the cooling channels of the magnets. This build up restricts the flow of cooling water and lowers the heat transfer

coefficient. The most effective treatment of this problem to date has been to flush the magnet cooling channels with a weak acid solution. In addition an effort has been made to minimize the amount of oxygen in solution in the cooling water system.

#### **IV. Acknowledgments**

The author would like to thank Frank Bieniosek, Mike Church, Elvin Harms, Jim Morgan, David Olivieri, Ralph Pasquinelli, and Dave Vander Meulen for much of the data relevant to antiproton source operation and for many helpful discussions. The author also acknowledges the efforts of the accelerator division operations department for their superb skill in operating the Fermilab accelerator complex and for much useful dialog during the course of the Run regarding the optimal way of operating the collider.

#### **V. References**

1. S. Shukla, Proceedings of the 1994 Meeting of the APS Division of Particles and Fields, University of New Mexico, 1485 (1994).
2. F.M. Bieniosek, K. Anderson, and K. Fullett, Requirements for a Beam Sweeping System for the Fermilab Antiproton Source Target, Submitted to the proceedings of the 1995 Particle Accelerator Conference, Dallas, TX, May (1995).
3. D. Olivieri, M. Church, and J. Morgan, A Dynamic Momentum Compaction Factor Lattice in the Fermilab Debuncher Ring, Submitted to the proceedings of the 1995 Particle Accelerator Conference, Dallas, TX, May (1995).
4. Fermilab, Design Report Tevatron I Project, section 5.9, September (1984).
5. R. Pasquinelli, private communication.
6. D. Vander Meulen, private communication.
7. K. Bertche, private communication.
8. F. M. Bieniosek, Emittance growth in recent antiproton transfers from the Accumulator to the Main Ring, Antiproton source departmental memo in preparation, September (1995).
9. S. Werkema, Control of Trapped Ion Instabilities in the Fermilab Antiproton Accumulator, Submitted to the Proceedings of the 1995 Particle Accelerator Conference, Dallas, TX, May (1995).